Chemical modification strategies for the control of graphene localization in PS/PMMA blend

Thibaut Lalire, A. Taguet, Jean Claude Roux, Belkacem Otazaghine, Claire Longuet

Chemical modification strategies for the control of graphene localization in PS/PMMA blend

Thibaut Lalire, Aurélie Taguet *, Jean-Claude Roux, Belkacem Otazaghine, Claire Longuet

Polymers Composites and Hybrids (PCH), IMT Mines Ales, Ales, France

A B S T R A C T

This work concerns the nanoparticles localization control in a PMMA/PS polymer blend. In this article, a complete study was made on the poly(methylmethacrylate)/polystyrene/graphene (PMMA/PS/graphene) polymer blend nanocomposites performed by a melt-blending process at PMMA/PS equal proportion (50/50). Graphene nanoparticles were modified via different chemical modification strategies such as Hummers' oxida-tion (GOxH), hydrazine reduction (GOxH-r_2) and copolymer functionalization by a "grafting onto" method. The evolution of graphene nanoparticles morphology, chemical structure during the melt-blending process were investigated to explain their final localization. Considering GOxH nanoparticles, the in-situ reduction during the process was proved by Raman spectroscopy, FTIR and XRD. The stability of the copolymer grafting was also confirmed after melt-compounding by Py-GC/MS. The predicted localization by thermodynamics was compared to the real localization determined by STEM images. Functionalized graphene (GOxN-PMMA, GOxH-PMMA, GOxH-r_2-PMMA, GOxH-r_2-PMMA-r_1) showed a transfer from PS to PMMA, whereas non-functionalized nano-particles (G, GOxH, GOxH-r_2) remain in PS. Graphene migration mechanisms and polymer blend microstructures were also investigated. Graphene nanoparticles interaction with polymer matrices and their impact on viscosity was studied by rheology to assess the final microstructure of the polymer blend nanocomposites.

Keywords:
Graphene
Chemical modification
Functionalization
Polymer blend
Localization

1. Introduction

Nanoparticles incorporation in polymer matrix became essential due to the need to improve polymer properties. Several types of carbon particles were attempted to improve electrical, mechanical and thermal properties. Graphene displayed interesting results in lots of applications such as energy storage, aeronautic, biomedical and appears as a promising 2D materials for the incorporation in polymer matrices [1–6]. Its high specific surface area, lightness and mechanical, thermal, electrical properties allow the production of performant nanocomposites.

Nanocomposites preparation is a real challenge, and several methods were tested as solvent casting, in-situ polymerization and melt blending [7]. At industrial scale, melt blending appears as the most appropriate process. Materials are incorporated in an extruder at high temperature with high shear force to mix and disperse reinforcing nanoparticles in polymer matrices. The interest of this method is the possibility to produce, in continuous cycle, high quantity of nanocomposite. *Macosko et al.* interestingly analyzed and reported the percolation threshold of nanocomposites bearing graphene in different matrices and for different processes [8]. And, solvent casting and in-situ polymerization methods allow to achieve nanocomposites with higher performance and lower amounts of graphene than the melt-blending process because higher nanoparticles dispersion can be reached.

While using melt blending scalable process, an interesting way to reduce the percolation threshold for graphene nanocomposites is to localize the graphene nanoplatelets in one phase or at the interface of a co-continuous immiscible polymer blend [9]. This was firstly described by *Sumita et al.* in 1991 [10], then in 1995 by *Gubbels et al.* [11,12] for carbon blacks and more recently, deeply explained by *Pötschke et al.* [13,14] for carbon nanotubes. *Pötschke et al.* [13,14] interestingly summarized the transfer speed of different nanoparticles through the PC/SAN interface of a co-continuous blend. Graphene and graphite are classified in intermediate and slow transfer, respectively, due to their intermediate and low aspect ratio. *Mao et al.* [15] showed that by dispersing an octadecylamine-functionalized graphene (GE-ODA) in the PS phase of a co-continuous PS/PMMA polymer blend, it is possible to decrease the percolation threshold to 0.5 wt%. The concept of double percolation is described by those authors as the localization of the

* Corresponding author.
E-mail address: aurelie.taguet@mines-ales.fr (A. Taguet).

nanoparticles at the interface of a co-continuous polymer blend. And it is seen to dramatically decrease the percolation threshold. Nevertheless, targeting the localization of NPs by controlling the migration and dispersion of graphene nanoparticles in polymeric matrices is still a big challenge [2].

As predicted by the wetting parameter, *Shen et al.* [16] were allowed to localize a reduced graphene oxide (rGOs) at the interface of a co-continuous EVA/PLA blend and reduce the percolation threshold to 0.18 wt%. However, in the literature, the double percolation was mainly obtained by playing on the melt process parameters [17]. *Mun et al.* [8] firstly dispersed graphene in the non-preferred PLA phase and then added the preferred HDPE phase. By these sequences of mixing the graphene was mainly dispersed at the interface of the co-continuous PLA/HDPE blend. Then, they were allowed to obtain an ultralow percolation threshold at 0.1 %vol. In the same manner, *Bai et al.* [18] dispersed graphene nanoplatelets (GNPs) at the interface of a co-continuous PS/PLA blend although the wetting parameter predict that GNPs should be localized in the PS phase. To achieve the GNPs trapping at the interface, they control the melt-compounding sequences, mixing times and shear rates. *Kou et al.* [19] described almost the same experiments while trapping GNPs at the interface of a co-continuous PLA/EVA blend. They also proved that while GNPs leave PLA quickly during initial compounding, they are trapped for a long time (2 to 10 min) at the interface. This leads to an electrical conductivity of 10^{-7} S/cm for a percolation threshold at 0.048 wt%. The authors defended that this value falls in the range of electrostatic discharge protection materials (10^{-4}–10^{-11} S/cm).

Other parameters than kinetics processing parameters play a key role in the dispersion and localization of graphene nanoplatelets in polymer blends, such as the polymer viscosity ratio, nanoparticle aspect ratio and size, and nanoparticle surface chemistry.

Graphene chemical modifications are sometimes operated before incorporation in a polymer matrix to avoid graphene nanoparticles aggregation and improve graphene/polymer interaction. These treatments tend to alter both graphene structure and electrical properties. In this case, a compromise between chemical modifications and electrical properties has to be found as demonstrated in our previous article [20].

In this previous article [20], different chemical treatment strategies have been investigated and the electrical conductivity of the nanoparticles has been measured. Generally, the higher the oxidation rate of the graphene, the lower the electrical conductivity. This demonstrates the necessity to reduce the graphene oxide nanoparticle in order to recover interesting electrical conductivity. It was shown that this reduction step can be performed by increasing the temperature to 250 °C or by a treatment with hydrazine. Thermal reduction can then be performed during the melt mixing process if the operating temperature is at least equal to 250 °C.

Finally, by analyzing the literature, it can be noticed that the influence of the chemical surface modification of graphene nanoparticles on their localization in a polymer blend, and by extension on the electrical conductivity, while using scalable melt mixing process, are rarely studied. In the present article, the selective localization of modified graphene particles in a polystyrene/poly(methylmethacrylate) (PS/PMMA) blend was studied. Several modified graphene samples, obtained using different strategies as described in our previous article, were used [20]. The influence of the modification of graphene chemical surface on the localization in the PS/PMMA immiscible polymer blend was investigated. The coherence between the real localization and that predicted by the thermodynamic coefficient (wetting parameter) was investigated.

2. Materials and method

2.1. Raw materials

Graphene KNG 180 (Xiamen Knano), Nitric acid (Sigma Aldrich), Sulfuric acid (Sigma Aldrich), Potassium permanganate (Sigma Aldrich), Hydrogen peroxide (33%) (Panreac), Hydrochloric acid (37%) (Panreac), PMMA Altuglas V825T (ARKEMA), PS Edistir (VERSALIS).

2.2. Synthesis of grafting agent P(MMA-co-HEMA)

The synthesis of the poly(methyl methacrylate-co-hydroxyl ethyl methacrylate) was described in a previous study [20] and consisted of a radical copolymerization of methyl methacrylate (MMA) and 2-hydroxyethyl methacrylate (HEMA) with a molar ratio MMA/HEMA = 95/5. Into a 100 mL flask fitted with a condenser, 10 g (0.1 mol) of MMA, 0.68 g (5.2×10^{-3} mol) of HEMA, 0.16 g (9.7×10^{-4} mol) of AIBN and 20 g of acetonitrile were introduced. Argon was bubbled through the mixture for 15 min. Then the mixture was stirred and heated at 80 °C for 3 h. After reaction, the copolymer (P(MMA-co-HEMA)) was purified by precipitation in methanol. The copolymer polydispersity index of 1.47 was determined by GPC (PMMA standard) with a M_n of 35000 g.mol^{-1}.

2.3. Oxidized graphene and polymer functionalized graphene

Graphene was modified via different chemical treatment strategies presented in our previous study [20]. Graphene was treated with two strategies called “soft” and “strong” with a first oxidation step based on nitric acid and Hummers’ methods, respectively. Then, hydrazine reduction was necessary to recover electrical property for the “strong” strategy after Hummers’ oxidation. Functionalization consisted in grafting the P(MMA-co-HEMA) copolymer (by esterification) on graphene oxide. Table 1 lists the powder samples prepared by different chemical strategies and Table 2 lists their characteristics.

2.4. Nanocomposites preparation

There are two types of final nanocomposite formulations: (1) graphene and modified graphene dispersed in a single polymer matrix (PS or PMMA) and (2) graphene and modified graphene dispersed in a PS/PMMA blend. Both were processed by solvent casting followed by melt mixing. The solvent casting step allows to facilitate the incorporation of

Table 1
List of the modified graphene samples, the different treatments used and the type of notation chosen. Referred to [20].

Materials	
G	Graphene
GO-PMMA	Oxidized graphene functionalized with P(MMA-co-HEMA)
Chemical, thermal treatments	
OxH	Oxidation using the Hummers’ method
OxN	Oxidation using nitric acid
r_1	Thermal reduction at 250 °C
r_2	Reduction using hydrazine hydrate
Sample examples	
GOxH-r_2	Hydrazine reduction of GOxH
GOxH-r_2-PMMA	*Steps:* Step 1: Hydrazine reduction of GOxH Step 2: functionalization with P(MMA-co-HEMA)
GOxH-PMMA-r_2	Step 1: functionalization of GOxH with P(MMA-co-HEMA) Step 2: Hydrazine reduction
GOxH-r_2-PMMA-r_1	*Step:* Step 1: Hydrazine reduction on GOxH Step 2: functionalization with P(MMA-co-HEMA) Step 3: Thermal reduction at 250 °C

Table 2
Physical characteristics of the different powder samples. Referred to [20].

Materials	Layer numbers[(1)]	Defects rate (I_D/I_G)[(2)]	Resistance (Ω)[(3)]
G	46–47	0.23	50
GOxH	9–10	1.03	No signal
GOxN	44–45	0.27	100
GOxH-PMMA	–	1.25	No signal
GOxN-PMMA	44–45	0.24	2566
GOxH-r_2	8	1.35	1067
GOxH-r_2-PMMA	–	1.38	6113
GOxH-r_2-PMMA-r_1	–	–	1203

[(1)]The number of layers was obtained by XRD.
[(2)]The rate of defects was obtained by Raman spectroscopy.
[(3)]The electrical resistance of the powders was obtained by a four probes installation.

the nanoparticles during the melt mixing. The solvent casting consisted in a premixing of graphene samples with PS or PMMA matrices using THF as a solvent. This step is called "masterbatch" and was performed on 2.5 g of compound (polymer matrix + nanoparticle). After THF evaporation, this masterbatch was added to polymer pellets into a micro-compounder DSM Xplore apparatus during the melt mixing step. The mixing parameters were fixed at 80 rpm, 250 °C and 4 min of mixing. 9.5g of polymer pellets were added to the masterbatch to get 12g of compound at the end. Polymers in the blend were incorporated at equivalent mass (50/50). Final polymer blends (PS/PMMA) nanocomposites were filled with 2 wt% of nanoparticles. Table 3 lists the polymers and nanocomposites

Procedure of extraction of nanoparticles was carried out on some nanocomposite formulations to characterize nanoparticles after the melt-compounding step. Hence, nanocomposite sample prepared as explain above, was introduced in THF during 3 days at 50 °C to remove all polymer matrix (PS or PMMA). Then nanoparticles and liquid phase were separated using centrifugation and the solid phase was washed 3 times with THF and 1 time with acetone. The obtained powder corresponding to the graphene particles was dried under vacuum for two days. Those samples are named "GOxH extracted".

Graphene and modified graphene dispersed in a single polymer matrix (PS or PMMA) were characterized by XRD, FTIR, py/GC–MS and rheology (refer to Table S1 in the supporting information). Graphene and modified graphene dispersed in the PS/PMMA blend were characterized by SEM.

2.5. Characterizations

FTIR spectra were recovered on a BRUKER Vertex 70 spectrometer to evaluate the oxidation state of the treated graphene samples by using ATR process. Spectra were obtained with a resolution of 4 cm^{-1} at room temperature in a wavenumber range between 4000 cm^{-1} and 400 cm^{-1}. XRD was used to get information about the structural changes on pristine and modified graphenes. The diffractometer used for these analyses is a BRUKER D8 Advance apparatus with a Cu Kα radiation (λ = 0.1542 nm). Raman spectroscopy was performed with a RENISHAW machine to analyze presence of defects in graphene structure before and after chemical modifications. The laser source used was 532 nm.

Contact angle measurements were carried out in order to determine surface tension, interfacial tension and wetting parameter to predict nanoparticles localization in the polymer blend. Water and diiodomethane drops were deposited with a controlled volume on the sample surface to determine polar and dispersive components, respectively. The contact angle between the drop and the substrate was measured using a KRÜSS Drop Shape Analyzer DSA30 goniometer apparatus. Each powder samples were produced by compression molding. The deposition of water and diiodomethane drops was performed three times on different sample zones. The dispersive (γ_S^d) and polar (γ_S^p) contributions to the surface energy of samples were calculated according to Eq. (1) using the Owens-Wendt model:

$$\gamma_L(1+\cos\theta) = 2\sqrt{\gamma_S^d\gamma_L^d} + 2\sqrt{\gamma_S^p\gamma_L^p} \quad (1)$$

Pyrolysis–gas chromatography–mass spectrometry (Py-GC/MS) analytical setup consisted of an oven pyrolyzer connected to a GC/MS system. A pyrolyzer equipped with an electrically heating platinum filament (Pyroprobe 5000 from CDS Analytical) was used for the pyrolysis step under helium. Each sample (<1 mg) was introduced in a quartz tube between pieces of quartz wool. A coiled probe enabled the pyrolysis of the whole. The sample was heated directly at 900 °C (during 15 s) before gases formed during pyrolysis were drawn to the gas chromatograph (during 5 min). The pyrolyzer apparatus is connected to a gas chromatograph (450-GC from Varian) by means of a transfer line heated at 270 °C. The GC initial temperature of 70 °C was held for 0.2 min, and then raised to 310 °C at 10 °C/min. The Varian Vf-5 ms capillary column (30 m × 0.25 mm) used for separation was under helium (1 mL/min) with a split ratio set to 1:50. After separation, the pyrolysis products were introduced to the ion trap analyzer of the 240-MS mass spectrometer (Varian) through the direct-coupled capillary column. The NIST mass spectral library was used to identify the pyrolysis products.

STEM micrographs were performed with an Environmental Scanning Electron Microscope equipped with Energy Dispersive X-ray spectroscopy (ESEM–EDX) (Quanta 200 FEG) from the FEI Company. A STEM detector composed of two diodes named (A and B) and 8 positions was added to the system. This set up is also called "STEM-in-SEM". The observed composites were prepared by ultramicrotomy at ambiant temperature on extruded samples. Nanocomposite slices obtained were around 40 nm thick and were placed on a STEM grid support. STEM images were realized from two methods: "Dark field" or "Bright field" also named DF or BF, respectively. According to the sample position and the diode used to receive electrons, DF or BF images can be obtained. DF is for diffused electron and BF for transmitted electron. By switching from one field to the other, the image contrast is reversed as demonstrated in Fig. S1. Knowing in which field images are performed is important in the case of immiscible polymer blend system. In our study, bright field were used. Hence, samples were always put in position B and the data were collected by diode B.

Rheological measurements were carried out with a MCR 702 Anton Paar apparatus at 250 °C in a frequency range from 100 to 0.1 rad/s and under nitrogen. The samples were disks of polymer blend filled with graphene or modified graphene obtained by injection molding. The applied strain was 0.9 % in order to do the frequency sweep in the linear viscoelastic domain.

Table 3
List of the polymers and nanocomposites.

Polymers	
PS (Edistir)	PS, η_0 = 95 Pa.s
PMMA V825T	PMMA, η_0 = 1244 Pa.s
Nanocomposites sequences example	
(G/PS)/PMMA	Step 1: Masterbatch of G/PS
	Step 2: Masterbatch mixed with PMMA by melt-compounding

3. Results and discussion

3.1. Morphology and chemical structure evolution of modified graphene particles during the melt-compounding

3.1.1. In-situ reduction of oxidized graphene during the melt-compounding

Firstly, XRD diffractogram of GOxH was compared to that of graphene and shows a complete modification, with the presence of a peak at

10.4° for GOxH assigned to an increase of the interlayer distance between sheets due to the intercalation of functional groups (Fig. 1a). Moreover, an enlargement of the peak is also observed, which corresponds to the delamination of graphene sheets.

Oxidized graphene from Hummers' method (GOxH) is considered as an electrical insulating material [20]. To improve electrical property of the final nanocomposite it is necessary to reduce the graphene oxide (GO) to recover a graphene-like sp^2 conductive structure. Reduction of GO can occur at around 200 °C [20]. Knowing that the processing temperature to produce the nanocomposite based on PMMA and GO or GOxH is 250 °C, we assume that a large part of the oxygenated groups should decompose during the extrusion step.

In order to confirm this hypothesis, the GOxH particles were extracted from PMMA after the melt-compounding step, to analyze the arrangement of graphene sheets.

After melt-compounding at 250 °C and THF extraction, a peak at 26.2° similar to the one observed on the graphene diffractogram is present. This evolution was attributed to a restacking of GOxH sheets due to a reduction reaction in the polymer matrix during the extrusion step at 250 °C. The elimination of these functional groups and the recovery of the sp^2 structure led to a reactivation of the Van der Waals interactions between π-π bonds of graphene sheets. In Fig. 1a, a broad peak is observed for GOxH/PMMA at 20° corresponding to the amorphous part of PMMA matrix. Three peaks at 21°, 24° and 26.4° are also present and correspond to different interlayer spacing of graphene sheets. These different peaks are probably due to an inhomogeneous reduction degree of GOxH nanoparticles that led to different interlayer distances. In all cases, this XRD result confirms that there is a thermal reduction of GOxH during the melt process that makes the restacking of graphene sheets possible. Moreover, FTIR analysis (Fig. 1b) confirms also the reduction of GOxH during the extrusion process with the disappearance of the large band at 3500 cm^{-1} corresponding to –OH bonds. The band at 1250 cm^{-1} characteristic of C-O bonds does not appear also for extracted GOxH. Raman spectroscopy (Fig. S2) confirmed as well the reduction of GOxH with a full width at half-–maximum (FWHM) decrease for the D band (FWHM from 148 cm^{-1} to 126 cm^{-1} for GOxH and GOxH/PMMA, respectively) and the G band (FWHM from 100 cm^{-1} to 82 cm^{-1} for GOxH and GOxH/PMMA, respectively) [21]. The shift of G band at lower Raman shift, (from 1600 cm^{-1} for GOxH to and 1596 cm^{-1} for GOxH/PMMA) also confirmed the thermal reduction after melt blending. This point is deeply explained in reference [20].

Hence, a restacking of GOxH sheets occurs during the melt-process and that is due to the elimination of one part of the oxidized groups. This can be identified as a partial reduction step.

3.1.2. Stability of the grafted P(MMA-co-HEMA) chains during the melt-compounding process

The grafting of P(MMA-co-HEMA) onto GOxH (leading to GOxH-PMMA) was described in our previous article [20]. To verify the presence of the grafted copolymer chains even after the melt compounding process, GOxH-PMMA was incorporated into a PS matrix using the extrusion process and then the functionalized graphene particles were extracted from the polymer using THF, as described previously.

Considering that graphene sheets were dispersed in PS matrix, the detection of methyl methacrylate molecules by Py-GC/MS analysis, from extracted GOxH-PMMA particles, can be attributed only to the grafted P(MMA-co-HEMA) copolymer chains. The comparison of GOxH-PMMA and extracted GOxH-PMMA chromatograms in Fig. 2 shows several differences which were attributed to the in-situ reduction of one part of the oxygenated groups during the melt-process (as shown previously for GOxH). Indeed, this reduction reaction involves modification of chemical composition for graphene nanoparticles which modifies their decomposition behavior during the pyrolysis step and therefore the nature of the obtained products. Moreover, the presence of toluene in

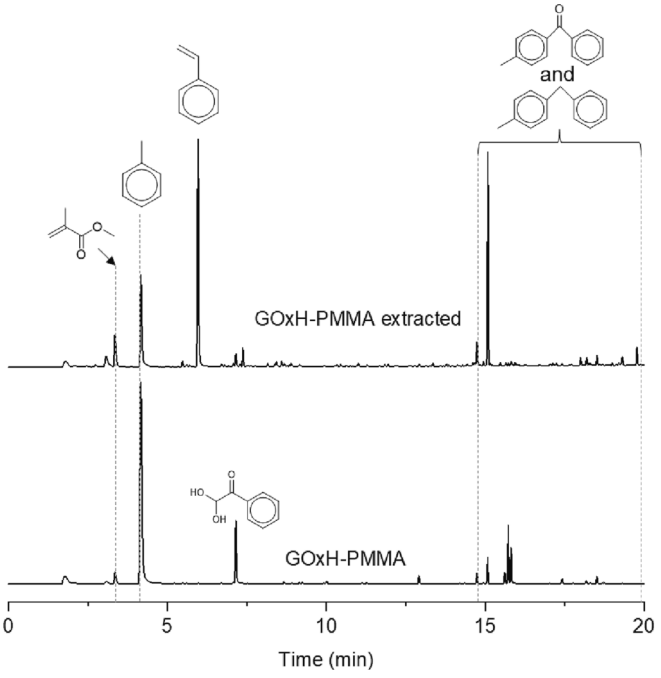

Fig. 2. Py-GC/MS of GOxH-PMMA and GOxH-PMMA after melt compounding with PS matrix and elimination of PS phase.

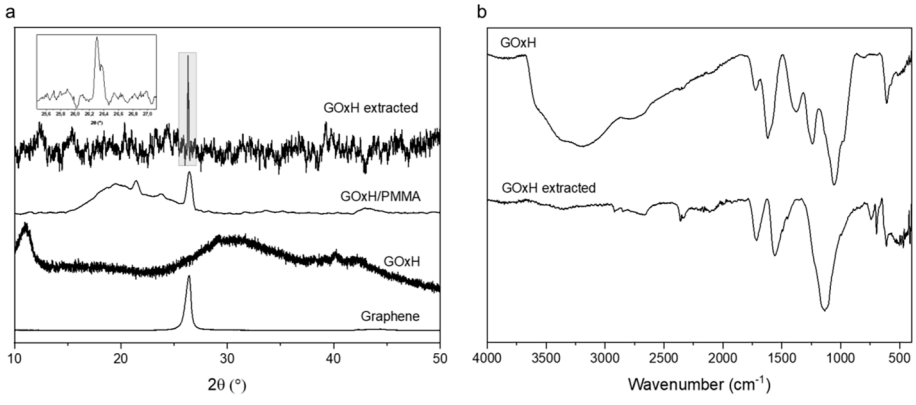

Fig. 1. (a) XRD of graphene, GOxH, GOxH dispersed in PMMA (GOxH/PMMA disk) and GOxH extracted from the PMMA matrix (GOxH extracted) with the framed peak at 26.2°, (b) FTIR spectra of GOxH and GOxH extracted.

high quantity for GOxH-PMMA was attributed to the trapping of solvent molecules between sheets during the functionalization step. Styrene molecules are predominant in the chromatogram of GOxH-PMMA after extraction. This was attributed to the presence of PS matrix chains that were not completely dissolved and eliminated during the extraction procedure.

Hence, a lots of similar products are seen in chromatograms before and after extrusion step but their proportions change significantly (Fig. 2). Especially, the methyl methacrylate peak proves the stability of the copolymer grafting during the melt process.

3.1.3. Rheological analysis of the different graphenes into PS or PMMA matrices

Rheological behavior and especially dynamic oscillatory experiments, is an interesting tool to characterize the dispersion state of nanoparticles into a polymer matrix.

Fig. 3a and b reports the evolution of the complex viscosity versus frequency for each nanoparticle dispersed in each PS or PMMA polymer phase.

Fig. 3a and b shows that PS and PMMA viscosities decrease with graphene (G) incorporation.

Einstein theory [22] described the increase of the viscosity of a matrix as a function of the volume fraction of fillers. By extension, non-Einstein behavior describes the viscosity drop when adding fillers. The "Non-Einstein" like phenomenon takes into account the nanoparticle radius and the polymer chain gyration radius [23]. Viscosity reduction was often described when graphene or graphite were introduced into polymers [16]. In their work, *Merkel et al.* [24] attributed the decrease of the viscosity for a nanocomposite to excluded free volume induced around the nanoparticles. Other works explained the viscosity decrease of PS when adding graphene or graphite to the π-π interaction between the aromatic cycle of styrene units and graphene sheets. Moreover, the low surface friction of graphene favors interfacial slippage between nanoparticles and polymer matrices and also tend to decrease the viscosity at low filler concentration [25]. This phenomenon was also demonstrated with the compact nature of crosslinked PS nanoparticles dispersed in a PS matrix which induced reduction of local friction and disentanglement of bulk polymer chains [26]. Lower local friction resulted in viscosity reduction. For PMMA, viscosity decreases also after the graphene incorporation probably due to the same slippage phenomenon (Fig. 3a). The commercial graphene is made of particles containing around 45 layers (Table 2) with a high rigidity and a compact nature of stacking sheets [27,28]. This structure favors the slippage of polymer chains. Moreover, graphene is known for its lubricant characteristic which can explain the viscosity reduction of polymers [29]. On the contrary, with GOxH, viscosities are higher than for neat polymer matrices. Hummers' method decreases the number of graphene layers that goes from around 45 for neat graphene (G) to around 9–10 layers for GOxH (Table 2); and the rigididy of the particles is decreased. Hence, the oxidized nanoparticles are more flexible with a wrinkled surface which allows polymer chains entrapping and adsorption [30]. Nanoparticle higher aspect ratio tends to increase nanocomposite viscosity [30] and in our case, aspect ratio of GOxH is higher than the commercial graphene. *Colonna et al.* explained that highly expanded and wavy nanoparticles, as our graphene oxide (GOxH), favors polymer chains impregnation between flakes which led to viscosity increase all along the frequency sweep [31].

Regarding the reduction of GOxH with hydrazine (GOxH-r_2), PS filled with these nanoparticles led to a viscosity decrease compared to neat PS or GOxH/PS. After hydrazine reduction, the layer number for GOxH-r_2 particle is around 8 (Table 2) but a sheet restacking is seen with the partially recovered structure of graphene (Fig. S3). This is due to the decomposition of one part of the oxygenated groups. This reduction reaction results in an interlayer distance decrease which reduces the probability of polymer chains intercalation and increases the rigidity of the particle. It explains the viscosity reduction for PS compared to nanocomposite mixed with GOxH. Nevertheless, since GOxH-r_2 is more flexible than G and contains more oxygen groups than G, there is more surface friction than for graphene particles. This may explain that a higher viscosity is obtained for GOxH-r_2/PS compared to G/PS nanocomposite. About GOxH-r_2 in PMMA matrix, the viscosity is lower than GOxH/PMMA at low frequencies (<1 rad/s) probably due to the restacking of sheets which didn't permit the impregnation of polymer chains between graphene sheets. However, the viscosity is higher than the other formulations due to interaction of remaining oxygenated groups on GOxH-r_2 with the PMMA polymer chains.

When GOxH-PMMA is used, PS nanocomposite viscosity increases in comparison to neat PS matrix but stay lower than that of PS filled with GOxH. With the PMMA matrix, viscosity decreases after the incorporation of the functionalized GOxH-PMMA nanoparticles and is also much lower than for G/PMMA composite for which the rigidity of graphene is the reason of the viscosity drop. The same result was obtained with GOxN-PMMA/PMMA (GOxN was oxidized with nitric acid), as its viscosity was lower than G/PMMA nanocomposite. Knowing that the number of layers of G and GOxN-PMMA is identical (around 45 in Table 2), it proves that a lower viscosity for GOxN-PMMA/PMMA compared to G/PMMA is due to a different chemical surface of the nanoparticles and not to the rigidity or compact nature of the nanoparticles.

Jain et al. [32] described a PP/silica system for which high molar mass PP chains were physisorbed at the surface of the silica NPs while low molar mass constitutes the surrounding molten matrix. And this leads to a viscosity decrease. Indeed, physisorption of high molar mass PP results in a reduction in entanglement density in the bulk, therefore increasing the flowability or reducing the viscosity.

Hence, the difference of behavior regarding the incorporation of GOxH-PMMA in PMMA or PS can probably be explained by a difference of interaction between the macromolecules of PS or PMMA bulk and the

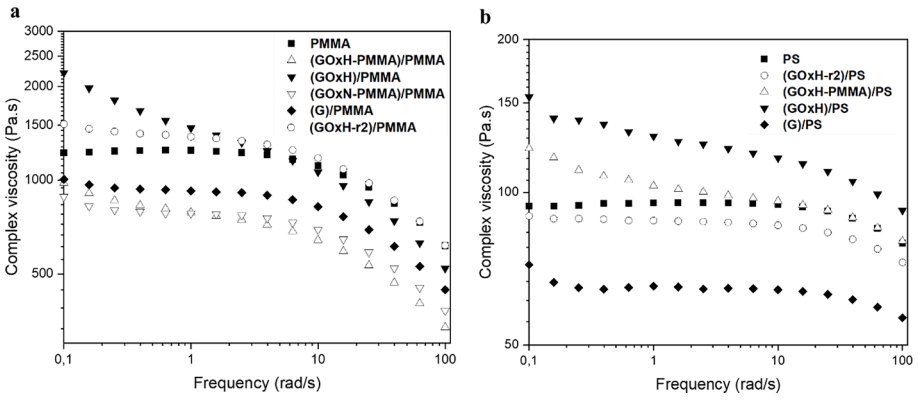

Fig. 3. Complex viscosities at 250 °C of (a) neat and filled PMMA and (b) neat and filled PS. 2 wt% of nanoparticles was incorporated.

PMMA chains grafted at the graphene surface. As in the work of *Jain et al.* [32], GOxH-PMMA dispersed in PMMA leads to physisorption of bulk PMMA chains at the surface of the functionalized graphene, reducing the entanglements in the bulk and the viscosity. This viscosity reduction for GOxH-PMMA in PMMA matrix can also be assigned to an autophobic dewetting behavior. This autophobic behavior was described by Kwon et al. [33] in the case of silica NPs grafted with high density of dopamine-modified poly(ethylene glycol) brush polymer and dispersed in a PEG matrix. They explained the rheological results (decrease of G' and G'' compared to the bare silica for low and moderate volume fraction of NPs) by a dewetting of bulk polymer chains that can not bridge the NPs due to a high amount of short (molar mass below the entanglement molar mass, M_e) brushes at the surface of the silica NPs [33,34]. This was previously also described by *Giovino et al* as an effect of chain mobility at the particle interface [35]. Whereas in the case of GOxH-PMMA dispersed in PS, no physisorption occurs, because there is no affinity between the PMMA grafted polymers and the PS chains and the viscosity is slightly increased.

3.2. Evolution of the graphene particle localization in the polymer blend

3.2.1. Contact angle measurements

The contact angle measurement technique is a suitable method to obtain surface energy of a material. The angle between the deposited drop and the surface can change according to the surface chemical composition. Effectively, Fig. 4 shows water drop on the surface of powder pellets obtained with different modified graphene samples. A variation of the contact angle can clearly be observed for these samples. In Table 4, relative surface energy of the modified graphene were determined thanks to Owens-Wendt method. Due to the oxidation reaction, graphene oxide nanoparticles are obviously the most hydrophilic and this is in accordance with a decrease of the contact angle with water. The decrease is mostly pronounced for GOxH due to the large presence of oxygenated groups. The soft oxidation by nitric acid method (GOxN) shows a less pronounced reduction of the contact angle. The grafting of the copolymer chains is also proved by a strong increase of the angle that reached 90° for GOxN-PMMA. The contact angle for GOxH-PMMA is lower than for GOxN-PMMA due to the large presence of oxygenated groups due to Hummer's oxidation and that were not removed after functionalization. The change in contact angle between oxidized (GOxH and GOxN) and functionalized graphenes (GOxH-PMMA and GOxN-PMMA) proves that the oxidized graphene surface become more hydrophobic after grafting. Finally, regarding the reduction step (r_2 or r_1), the grafting is maintained after the hydrazine reduction (r_2) leading to an increase of the contact angle and it is maintained even after the thermal treatment step (r_1). This is consistent with the previous part on the grafting stability proven after melt-compounding.

Table 4
Surface energy of graphene and modified graphene nanoparticles.

Materials	γ^d (mN/m) (25 °C)	γ^p (mN/m) (25 °C)	γ (mN/m) (25 °C)	$d\gamma/dT$ (mN/m/°C)
G	43.88	11.59	*55.47*	0
GOxH	40.24	22.15	*62.40*	−0.1 [36]
GOxH-r_2	46.53	6.43	*52.96*	0;-0.1 [36]
GOxH-PMMA	41.15	5.78	*46.93*	0
GOxN	44.95	14.28	*59.22*	0
GOxN-PMMA	44.71	0.51	*45.22*	0
GOxH-r_2-PMMA	43.27	1.00	*44.27*	0
GOxH-r_2-PMMA-r_1	45.05	0.02	*45.07*	0
PMMA	41.77	1.89	*43.66*	−0.077 [37]
PS	39.35	0.87	*40.22*	−0.072 [37]

3.2.2. Thermodynamic prediction of the localization of modified graphene particles

In polymer blends, the nanoparticle localization can be predicted by determining interfacial tension and calculating wettability coefficient (also called wetting parameter) based on thermodynamic prediction. Nanoparticles localization was determined according to the Young's equation (Eq. (2)) by obtaining the wettability coefficient:

$$\omega_a = \frac{\gamma_{np-PMMA} - \gamma_{np-PS}}{\gamma_{PS-PMMA}} \quad (2)$$

$\gamma_{np-PMMA}$ represents the interfacial energy between the nanoparticle and PMMA, γ_{np-PS} the interfacial energy between the nanoparticle and PS, $\gamma_{PS-PMMA}$ the interfacial energy between PMMA and PS. If:

- $\omega_a > 1$, nanoparticles are located in the PS phase
- $\omega_a < -1$ nanoparticles are located in PMMA phase
- $-1 < \omega_a < 1$ nanoparticles are located at the interface

By using surface energy determined with contact angle measurements, the interfacial tension can be calculated. Two methods were applied such as harmonic and geometric mean equations. Geometric mean equation (Eq. (3)) is preferred for filled polymers whereas, Harmonic mean equation (Eq. (4)) is preferred for neat polymers [38]. As some articles describe the use of both equations [39], Table 5 and Table 6 compare both.

$$\gamma_{12} = \gamma_1 + \gamma_2 - 4\left(\frac{\gamma_1^d \gamma_2^d}{\gamma_1^d + \gamma_2^d} + \frac{\gamma_1^p \gamma_2^p}{\gamma_1^p + \gamma_2^p}\right) \quad (3)$$

$$\gamma_{12} = \gamma_1 + \gamma_2 - 2\left(\sqrt{\gamma_1^d \gamma_2^d} + \sqrt{\gamma_1^p \gamma_2^p}\right) \quad (4)$$

γ_1 and γ_2 are the surface energies, γ_1^d *and* γ_2^d are the dispersive components, γ_1^p *and* γ_2^p are the polar components of materials 1 and 2,

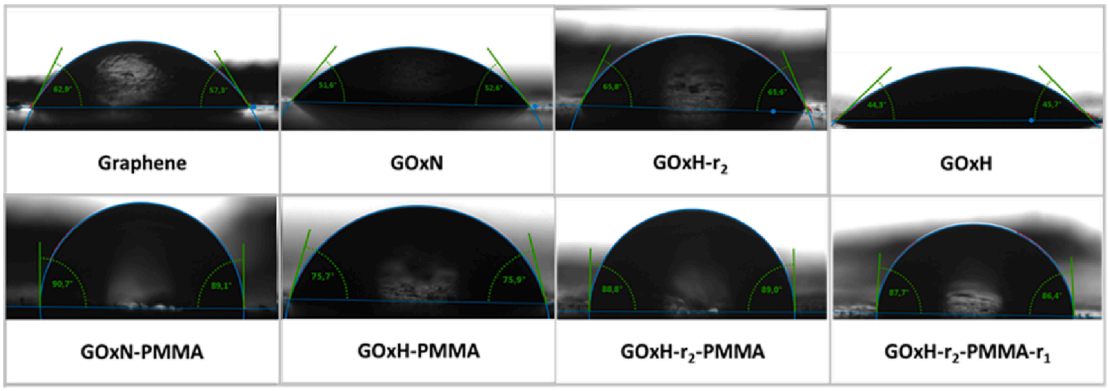

Fig. 4. Water contact angle measurement for different modified graphene samples.

Table 5
Wettability coefficient at 25 °C and prediction of fillers localization in PS/PMMA blend.

Materials	Wettability coefficient (from Harmonic) 25 °C	Wettability coefficient (from Geometric) 25 °C	Localization of the nanoparticles
G/PS/PMMA	−5,42	−9,01	PMMA
GOxH/PS/PMMA	−5.74	−13.52	PMMA
GOxH-PMMA/PS/PMMA	−3.75	−4.85	PMMA
GOxN-PMMA/PS/PMMA	1.00	1.15	**Interface-PS**
GOxH-r_2/PS/PMMA	−4.67	−6.02	PMMA
GOxH-r_2-PMMA/PS/PMMA	0.23	0.24	**Interface**
GOxH-r_2-PMMA-r_1/PS/PMMA	1.68	3.30	PS

Table 6
Wettability coefficient at 250 °C and prediction of fillers localization in PS/PMMA blend.

Materials	Wettability coefficient (from Harmonic) 250 °C	Wettability coefficient (from Geometric) 250 °C	Localization of the nanoparticles	REAL Localization
G/PS/PMMA	−9.12	−15.51	PMMA	PS
GOxH/PS/PMMA	−5.82	−13.62	PMMA	PS
GOxH-PMMA/PS/PMMA	−7.78	−10.39	PMMA	PMMA
GOxN-PMMA/PS/PMMA	−3.11	−3.18	PMMA	PMMA
GOxH-r_2/PS/PMMA	−4.15	−5.32	PMMA	PS
GOxH-r_2-PMMA/PS/PMMA	−4.20	−4.25	PMMA	Interface & PMMA
GOxH-r_2-PMMA-r_1/PS/PMMA	**−1.86**	**−0.58**	**Interface & PMMA**	Interface & PMMA

respectively. Wettability coefficient at 25 °C and 250 °C are listed in Table 5 and Table 6, respectively, according to Harmonic and Geometric mean equations. Localization of nanoparticles was also predicted. With the extrapolation at the melting temperature during the process, only GOxH-r_2-PMMA-r_1 is expected to be located at the interface between PS and PMMA.

3.2.3. Impact of graphene particle modification on their real localization

STEM images were used to characterize the graphene nanoparticles localization in the PS/PMMA blend. For the obtained STEM images, the lightest regions correspond to PMMA phase, the darkest to the PS phase. White parts are holes which were created during the ultramicrotomy preparation of the samples. Table 6 is completed with a column mentioning the real localization (based on those STEM images) of the NPs in the blend after the melt processing. Pristine graphene seems to form agglomerates and remains in the PS phase after mixing. About GOxH nanoparticles, thermodynamics predicts (Tables 5 and 6) that, due to the strong oxidation, the particles should localize in the PMMA phase. However, as the GOxH was thermally reduced during the melt-blending process (which was confirmed *in 3.1.1*), the real final localization is in the PS. Indeed, this thermal reduction at 250 °C, leads to the decomposition of one part of the oxygenated groups which allows the recovery of a sp^2 structure and the formation of π-π interactions between the PS matrix and the graphene sheets. The same localization was observed for GOxH-r_2, that is localized in the PS matrix and not in the PMMA matrix as determined by the thermodynamic predictions. However, wettability coefficient values increase after hydrazine reduction (from −5.82 to −4.15 for GOxH and GOxH-r_2, respectively) which tend to a PS location. Hence, hydrazine reduction of GOxH nanoparticles allows to recover a part of the graphene-based structure and therefore possible π-π interactions between GOxH-r_2 and PS. Moreover the restacking of graphene sheets (Fig. S3), due to the hydrazine reduction, makes difficult the transfer to the PMMA phase. Moreover, if the thermodynamic prediction for localization of nanoparticles was not totally in accordance with the real localization it is probably due to the weak precision of contact angle measurement. Effectively, this method is sensitive to the roughness of the sample, the environment, and also to the porosity of the compressed powder. Moreover, the reliability of surface energy measurements by contact angle depends on several conditions and can be disturbed by the chemical composition evolution of oxidized graphene nanoparticles during the melt process. That's why it is difficult to assert the particle localization only on thermodynamic prediction.

Some studies analyzed the impact of the polymer viscosity ratio on particle localization. The conclusion of most articles was that, when mixed all together (polymers were first added and then particles were added), particles tend to remain in the polymer with the highest viscosity, whatever the chemical nature of the particles [38,40]. In our case, there are then two explanation for the final localization of GOxH and GOxH-r_2 in PS: (1) the sequence of mixing (GOxH and GOxH-r_2 are primarily dispersed in PS and PMMA is further added) plays a key role in the final localization because (2) the chemical structure of the nanoparticles has a strong impact on the localization since GOxH and GOxH-r_2 remain in the PS matrix which has the lowest viscosity compared to the PMMA phase.

By grafting with the copolymer chains, both GOxH-PMMA and GOxN-PMMA goes through the interface to the PMMA phase (Fig. 5a and c). In our previous study [20], the grafting density of GOxN-PMMA was determined to be much lower than that of GOxH-PMMA, due to the lower number of functional groups created on GOxN than GOxH. The lowest grafting rate of PMMA for GOxN-PMMA therefore seems sufficient to allow its migration to the PMMA phase during the processing. For GOxH-r_2-PMMA, one part of the nanoparticles seems to be located in the PMMA phase, which is the preferred phase, whereas others are also located at the interface. The same observations are performed for GOxH-r_2-PMMA-r_1 particles. GOxH-r_2-PMMA and GOxH-r_2-PMMA-r_1 seem to be the most promising nanoparticles for the dispersion in a co-continuous PS/PMMA polymer blend to get efficient electrical properties at low graphene amounts. As demonstrated previously by *Pötschke et al.* [14], the localization at the interface of a high aspect ratio nanoparticle (platelets, nanotubes) depends strongly on the dimension of the nanoparticles (lateral size) and the way they reach the interface (the larger the size of sheets, the longer it takes to pass through the interface). It was described as the slim-fast mechanism. Indeed, perpendicular orientation of sheets at the interface allows to migrate faster into the other phase [19]. The heterogeneous distribution in the length of this nanoparticle explains that some platelets have a longer stay at the interface whereas others (smallest) migrate faster through the interface.

There are some similarity between thermodynamic prediction and STEM images. The localization predictions are consistent with the experimental observations for GOxN-PMMA, GOxH-PMMA, GOxH-r_2-

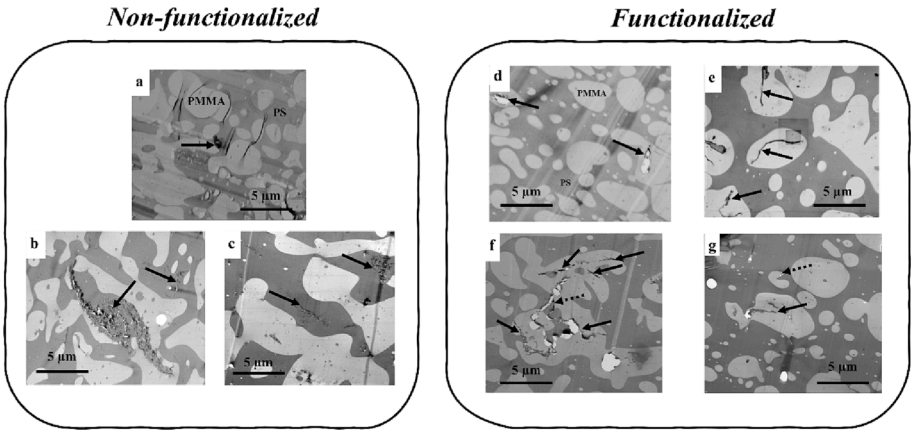

Fig. 5. STEM images of nanoparticles/PS/PMMA composites melt mixed at 250 °C with a pre-dispersion of nanoparticles in PS matrix by solvent-casting method. Nanocomposites of PS/PMMA filled with 2 wt% of (a) G, (b) GOxH,(c) GOxH-r_2, (d) GOxN-PMMA, (e) GOxH-PMMA, (f) GOxH-r_2-PMMA, (g) GOxH-r_2-PMMA-r_1. Black arrows indicate the presence of graphene nanoparticles and dashed arrows indicate interfacial graphene.

PMMA and GOxH-r_2-PMMA-r_1. For GOxH-r_2, GOxH and G, the predicted localizations are not in agreement with the obtained microstructures. As mentioned previously, it is assumed that this is due to the chemical structure evolution of the nanoparticles during the melt-compounding or the high rigidity of G. The stability of the copolymer grafting on graphene nanoparticles during the mixing showed also a strong impact on the localization of the fillers in the PMMA/PS polymer blend which makes possible the control of their localization.

3.2.4. *Polymer blend morphology evolution*

With the prospect of producing electrically conductive nanocomposites, a co-continuous morphology should facilitate the percolation of graphene particles, even for low filler rates. Polymer blend morphology depends strongly on polymer viscosity ratio. Moreover, for polymer blend nanocomposites, the presence of nanoparticles leads to viscosity variation according to the filler quantity. In this case, it is important to control the evolution of polymer viscosity due to the presence of nanoparticles and to determine the suitable concentration for each polymer phase to obtain a co-continuous morphology. The understanding of nanoparticles migration during the extrusion process is also necessary to control their localization and reach the percolation threshold.

For polymer blends, Paul and Barlow model [41] is a simple model that allows the prediction of phase inversion for two polymers A and B if their viscosities (η_A and η_B) and volume ratios (V_A and V_B) are known, as described by Equation (5).

$$\frac{V_A}{V_B} \times \frac{\eta_B}{\eta_A} = X \tag{5}$$

IfX <1, the polymer phase B is continuous; X>1, the polymer phase A is continuous; X=1, both phases are continuous (co-continuous morphology).

In the case of the 50/50 PMMA/PS, this model predicts that PS would be the continuous phase and PMMA the dispersed one, which is in accordance with the morphology of the unfilled polymer blend obtained (Fig. 6a). When graphene and modified graphene are added it is seen in Fig. 5 that some morphologies are changed from matrix/dispersed phase to co-continuous.

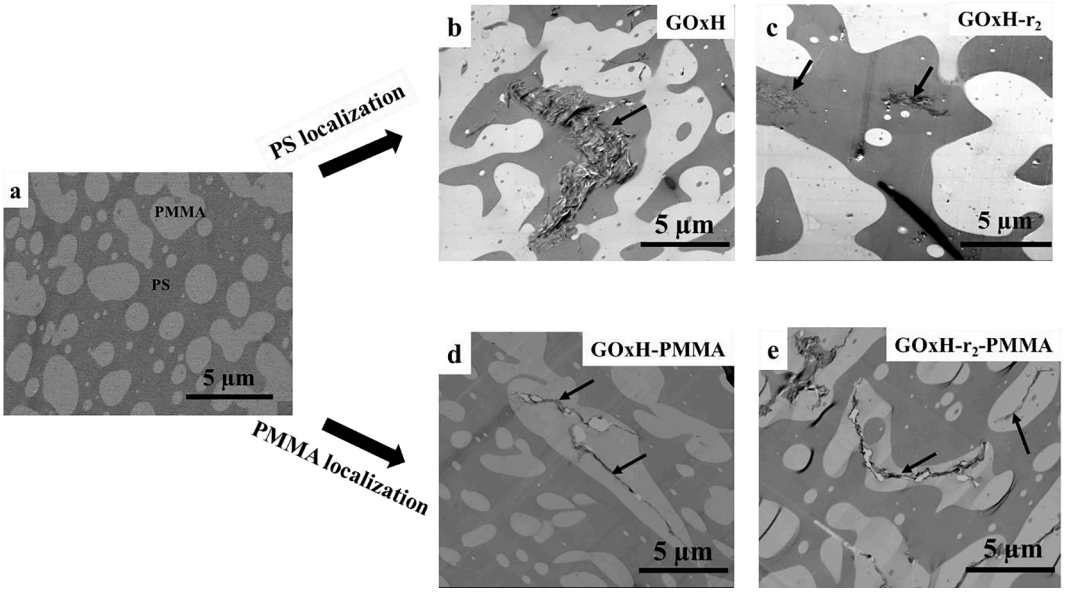

Fig. 6. STEM micrographs of polymer blend and polymer blend nanocomposites containing all 2 wt% of nanoparticles: (a) Neat PMMA/PS polymer blend, (b) GOxH/PS/PMMA, (c) GOxH-r_2/PS/PMMA, (d) GOxH-PMMA/PS/PMMA, (e) GOxH-r_2-PMMA/PMMA. Black arrows indicate nanoparticle.

3.2.5. Particles localization impact on nanocomposite microstructure

According to graphene modification strategy and extrusion procedure used, the nanoparticles migration and the evolution of the microstructure will be different in the PMMA/PS polymer blend. Neat 50/50 PMMA/PS polymer blend displays a PS matrix/ PMMA dispersed phase microstructure as seen in Fig. 6a and as predicted by Paul and Barlow model.

Native graphene and GOxH stay in the PS phase for different reasons. Native graphene remains in PS matrix due to the aggregate formation and also probably due to the compatibility with PS via π-π interaction. For GOxH, the in-situ reduction was proved in *§3.1.1,* this phenomenon led to decomposition of some oxygenated group which probably allow the recovery of affinity with PS matrix. This localization tend to increase the viscosity of the PS phase. Hence, the viscosity ratio between PS (+GOxH) and PMMA is increased and a co-continuous morphology is obtained (Fig. 6b).

Regarding GOxH-r_2 nanoparticles, the reason for their final localization in PS is also the π-π interaction (Fig. 5c). Hydrazine reduction decomposed a large amount of oxygenated groups. This localization led also to a co-continuous morphology due to viscosity ratio increase.

For GOxH-PMMA and GOxH-r_2-PMMA, nanoparticles are preferentially localized in PMMA phase, resulting in the formation of larger PMMA nodules (Fig. 6d and e). Effectively, nanoparticles with larger lateral size stretch the PMMA nodules and induce irregular shapes. This phenomenon can also lead to coalescence between these irregular PMMA nodules and favors the co-continuity. These mechanisms are described in Fig. 7.

3.2.6. Nanoparticles migration mechanisms during melt blending

For GOxH-r_2, nanoparticles tend to remain in PS phase. Due to the shear force during the compounding step, some sheets are located and stacked at the interface (Fig. 8a). The cutting effect by graphene sheets can occur [42] (Fig. 8a). The lack of affinity with PMMA leads to an encapsulation of GOxH-r_2. These nanoparticles are then trapped in small PS domains (Fig. 8b). This encapsulation was also proposed by *Bai et al.* [18] as a step migration for graphene located at the interface, before a transfer to the other phase for longer compounding times. The same encapsulation mechanism is observed for GOxH nanoparticles (Fig. S4).

About GOxH-PMMA, GOxH-r_2-PMMA and GOxH-r_2-PMMA-r_1, some nanoparticles are localized at the interface or in PMMA matrix as graphene particles have been premixed in PS phase. Nanoparticles premixed with the PS phase, with which they have the lowest affinity, tend to migrate in the preferred PMMA phase. As explained by *Macosko et al.* [19], graphene sheets tend to drain the PMMA/PS interface (Fig. 9). This time of migration depends on many parameters such as the contact distance between graphene nanoparticles and polymer interface. Effectively, nanosheets are transferred progressively in the PMMA phase (Fig. 8c). In general, for aggregates and particles with high lateral size, the transfer time from PS to PMMA is longer and can lead to an encapsulation mechanism. These mechanisms were described in Fig. 9.

4. Conclusion

In this study the chemical surface of graphene showed undeniably a strong impact on localization. The in-situ reduction of GOxH which changed its chemical composition during the melt-process allowed to explain why GOxH nanoparticles remained in the PS phase in PS/PMMA blend. On the contrary, nanoparticles grafted with PMMA chains (GOxH-r_2-PMMA and GOxH-r_2-PMMA-r_1) were localized in the PMMA phase or at the interface of PS/PMMA blends.

About rheological analysis, the influence of modified graphene nanoparticles on complex viscosity evolution is difficult to understand since several mechanisms can explain viscosity variations. By gathering information from the literature, some mechanisms were associated to

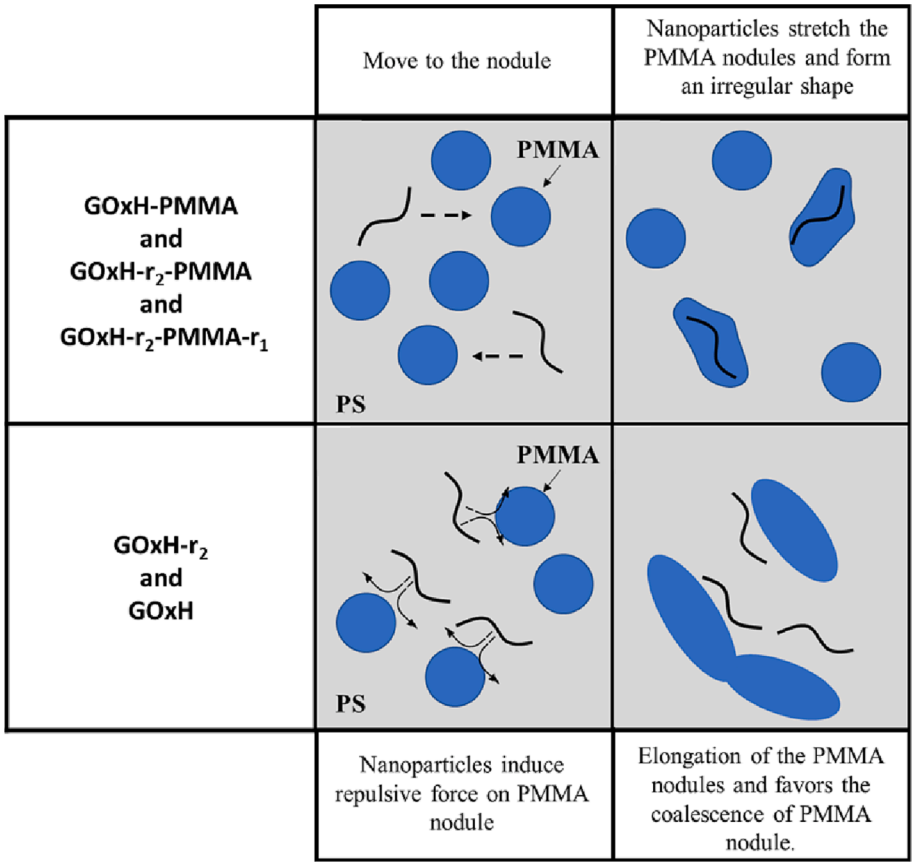

Fig. 7. Scheme of the morphology evolution in polymer blend nanocomposites.

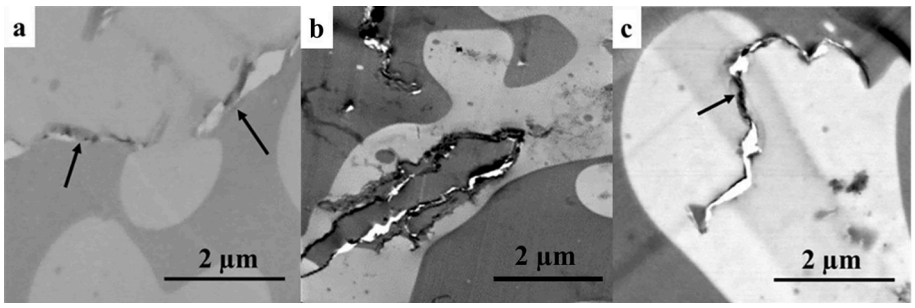

Fig. 8. (a) Cutting effect of GOxH-r_2 particles, (b) Encapsulation of GOxH-r_2 by a PMMA nodule, (c) Progressive transfer of GOxH-PMMA particle in a PMMA domain.

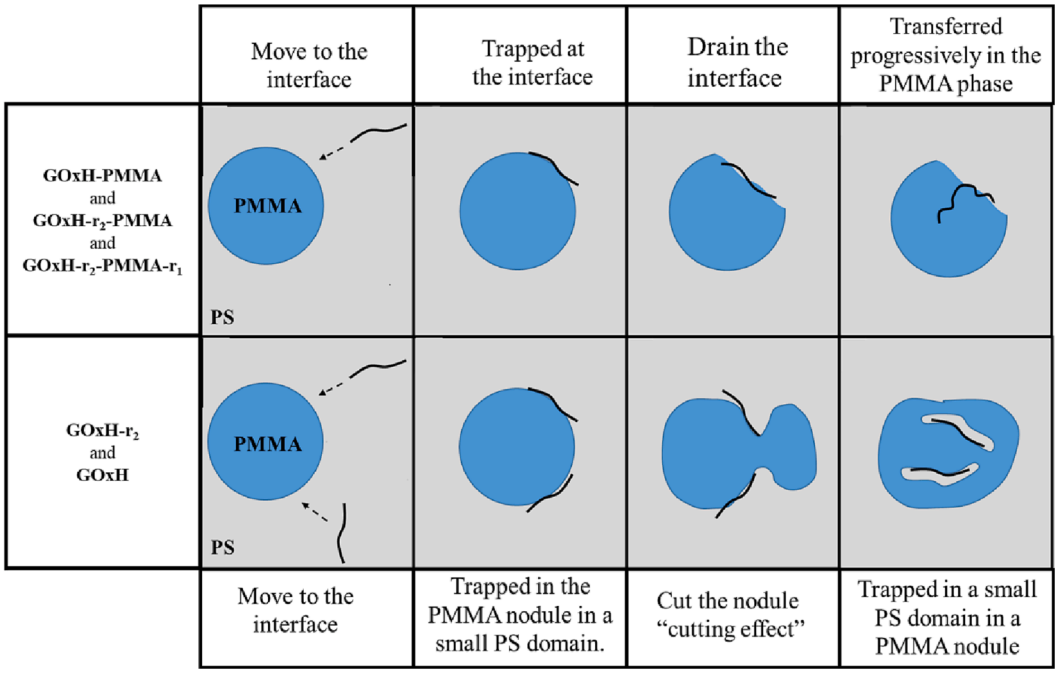

Fig. 9. Scheme of nanoparticles migration mechanisms.

our observations. Indeed, according to the number of layer and interlayer distance, graphene based nanoparticles can favor slippage phenomenon (viscosity reduction) or polymer chains impregnation between graphene platelets (viscosity increase). Influence of nanoparticle surface chemistry on viscosity was also discussed with functionalized graphene as an interesting viscosity variation occurred. The functionalization of graphene surface with PMMA copolymer chains dispersed in PMMA matrix resulted in a viscosity decrease. In our case, the surface functionalization resulted in a decrease of the entanglement density at the polymer-graphene interface probably due to a selective adsorption mechanism or to an autophobic dewetting.

For polymer blend morphology, the microstructure of the blend was switched from matrix/dispersed phase to co-continuous when NPs were added. For the samples for which the NPs were dispersed in the continuous PS phase, co-continuity was explained by a viscosity increase of the PS phase and a repulsion of the PMMA phases. Whereas, for the samples for which the NPs were dispersed in the PMMA phase or at the interface, co-continuity was explained by a delay in PMMA phase relaxation and a coalescence.

To produce performant nanocomposites, all aspects must be studied from nanoparticle synthesis to the nanocomposite preparation such as the nanoparticle properties, the nanoparticle structure evolution during the melt process, the morphology of the polymer blend system and also the control of the melt process parameters. All of these points will have an impact on final nanocomposite morphology and properties. By controlling the localization of graphene in a polymer blend, different applications appear. For nanoparticles localized in continuous phase, performant nanocomposite for EMI shielding or electrical sensors can be produced. For a localization in dispersed phase, dielectric material for nano-capacitor applications can be elaborated [43].

CRediT authorship contribution statement

Thibaut Lalire: Conceptualization, Formal analysis, Methodology, Investigation, Writing – original draft. **Aurélie Taguet:** Conceptualization, Validation, Formal analysis, Investigation, Writing – review & editing, Supervision. **Jean-Claude Roux:** Formal analysis. **Belkacem Otazaghine:** Conceptualization, Validation, Formal analysis, Investigation, Writing – review & editing. **Claire Longuet:** Conceptualization, Validation, Formal analysis, Investigation, Writing – review & editing, Supervision.

Declaration of Competing Interest

The authors declare that they have no known competing financial interests or personal relationships that could have appeared to influence the work reported in this paper.

Data availability

Data will be made available on request.

Acknowledgements

We gratefully acknowledge Vivien Truchot from INSA Lyon for the use of their microcompounder DSM Xplore. We want to thank the GDR (Groupe de Recherche) Polynano who was the provider of the graphene. Ecole Doctorale Sciences Chimiques Balard (Univ Montpellier) finances this work.

Appendix A. Supplementary data

Supplementary data to this article can be found online at https://doi.org/10.1016/j.flatc.2023.100500.

References

[1] V.B. Mohan, K.-T. Lau, D. Hui, D. Bhattacharyya, Graphene-based materials and their composites: A review on production, applications and product limitations, Compos B Eng 142 (2018) 200–220, https://doi.org/10.1016/j.compositesb.2018.01.013.

[2] D.N. Trivedi, N. v. Rachchh. Graphene and its application in thermoplastic polymers as nano-filler- A review. Polymer. 240. (2022). 124486. doi: 10.1016/j.polymer.2021.124486.

[3] B. Alemour, O. Badran, M.R. Hassan, A review of using conductive composite materials in solving lightening strike and ice accumulation problems in aviation, Journal of Aerospace Technology and Management. 11 (2019) 1–23, https://doi.org/10.5028/jatm.v11.1022.

[4] M. Silva, N.M. Alves, M.C. Paiva, Graphene-polymer nanocomposites for biomedical applications, Polym Adv Technol. 29 (2018) 687–700, https://doi.org/10.1002/pat.4164.

[5] M. Yusuf, M. Kumar, M.A. Khan, M. Sillanpää, H. Arafat, A review on exfoliation, characterization, environmental and energy applications of graphene and graphene-based composites, Adv Colloid Interface Sci 273 (2019) 102036, https://doi.org/10.1016/j.cis.2019.102036.

[6] F. Shen, D. Pankratov, Q. Chi, Graphene-conducting polymer nanocomposites for enhancing electrochemical capacitive energy storage, Curr Opin Electrochem 4 (1) (2017) 133–144, https://doi.org/10.1016/j.coelec.2017.10.023.

[7] W. Chen, H. Weimin, D. Li, S. Chen, Z. Dai, A critical review on the development and performance of polymer/graphene nanocomposites, Science and Engineering of Composite Materials. 25 (2018) 1059–1073, https://doi.org/10.1515/secm-2017-0199.

[8] S.C. Mun, M.J. Kim, M. Cobos, L. Gu, C.W. Macosko, Strategies for interfacial localization of graphene/polyethylene-based cocontinuous blends for electrical percolation, AIChE Journal. 65 (2019), 16579, doi:10.1002/aic.16579.

[9] B.o. Sun, F. Kong, M. Zhang, W. Wang, B.S. Kc, J. Tjong, M. Sain, Percolation model for renewable-carbon doped functional composites in packaging application: A brief review, Coatings. 10 (2) (2020) 19, https://doi.org/10.3390/coatings10020193.

[10] M. Sumita, K. Sakata, S. Asai, K. Miyasaka, H. Nakagawa, Dispersion of fillers and the electrical conductivity of polymer blends filled with carbon black, Polymer Bulletin 25 (2) (1991) 265–271, https://doi.org/10.1007/BF00310802.

[11] F. Gubbels, S. Blacher, E. Vanlathem, R. Jérôme, J.R. Deltour, O.F. Brouers, P. Teyssibt, Design of Electrical Conductive Composites: Key Role of the Morphology on the Electrical Properties of Carbon Black Filled Polymer Blends, Macromolecules. 28 (1995) 1559–1566.Doi: 10.1021/ma00109a030.

[12] F. Gubbels, R. Jbrome, P. Teyssib, E. Vanlathem, R. Deltour, A. Calderone, V. Parentb, J.L. Brbdas, Selective Localization of Carbon Black in Immiscible Polymer Blends: A Useful Tool To Design Electrical Conductive Composites, Macromolecules 27 (1994) 1972–1974, https://doi.org/10.1021/MA00085A049.

[13] A. Göldel, G. Kasaliwal, P. Pötschke, Selective localization and migration of multiwalled carbon nanotubes in blends of polycarbonate and poly(styrene-acrylonitrile), Macromol Rapid Commun. 30 (2009) 423–429, https://doi.org/10.1002/marc.200800549.

[14] A. Göldel, A. Marmur, G.R. Kasaliwal, P. Pötschke, G. Heinrich, Shape-dependent localization of carbon nanotubes and carbon black in an immiscible polymer blend during melt mixing, Macromolecules. 44 (2011) 6094–6102, https://doi.org/10.1021/ma200793a.

[15] C. Mao, Y. Zhu, W. Jiang, Design of electrical conductive composites: Tuning the morphology to improve the electrical properties of graphene filled immiscible polymer blends, ACS Appl Mater Interfaces. 4 (2012) 5281–5286, https://doi.org/10.1021/am301230q.

[16] Y. Shen, T.T. Zhang, J.H. Yang, N. Zhang, T. Huang, Y. Wang, Selective localization of reduced graphene oxides at the interface of PLA/EVA blend and its resultant electrical resistivity, Polym Compos. 38 (2017) 1982–1991, https://doi.org/10.1002/pc.23769.

[17] M. Liebscher, M.O. Blais, P. Pötschke, G. Heinrich, A morphological study on the dispersion and selective localization behavior of graphene nanoplatelets in immiscible polymer blends of PC and SAN, Polymer (Guildf). 54 (2013) 5875–5882, https://doi.org/10.1016/j.polymer.2013.08.009.

[18] L. Bai, R. Sharma, X. Cheng, C.W. Macosko, Kinetic Control of Graphene Localization in Co-continuous Polymer Blends via Melt Compounding, Langmuir. 34 (2018) 1073–1083, https://doi.org/10.1021/acs.langmuir.7b03085.

[19] Y. Kou, A.T. Cote, J. Liu, X. Cheng, C.W. Macosko, Robust networks of interfacial localized graphene in cocontinuous polymer blends, J Rheol (N Y N Y). 65 (2021) 1139–1153, https://doi.org/10.1122/8.0000294.

[20] T. Lalire, B. Otazaghine, A. Taguet, C. Longuet, Correlation between multiple chemical modification strategies on graphene or graphite and physical/electrical properties, FlatChem 33 (2022) 100376, https://doi.org/10.1016/j.flatc.2022.100376.

[21] I. Childres, L.A. Jauregui, W. Park, H. Cao, Y.P. Chen, Raman spectroscopy of graphene and related materials, in: New Developments in Photon and Materials Research, 2013.

[22] A. Einstein, Zur Theorie der Brownschen Bewegung, Ann Phys. 19 (1906) 248–258, https://doi.org/10.1002/andp.200590009.

[23] R. Eslami, S.R. Ghaffarian, M. Salehi, M. Rafizadeh, Evaluation of non-Einstein rheology behavior of soft nanoparticles/epoxy nano-composites and their multifunctional effects on curing kinetics, Polym Test. 66 (2018) 350–359, https://doi.org/10.1016/j.polymertesting.2018.02.007.

[24] T.C. Merkel, B.D. Freeman, R.J. Spontak, Z. He, I. Pinnau, P. Meakin, A.J. Hill, Ultrapermeable, Reverse-Selective Nanocomposite Membranes, Science 296 (2002) (1979) 519–522, https://doi.org/10.1126/science.1069580.

[25] E. Nilsson, H. Oxfall, W. Wandelt, R. Rychwalski, B. Hagström, Melt spinning of conductive textile fibers with hybridized graphite nanoplatelets and carbon black filler, J Appl Polym Sci. 130 (2013) 2579–2587, https://doi.org/10.1002/app.39480.

[26] E. Senses, C.L. Kitchens, A. Faraone, Viscosity reduction in polymer nanocomposites: Insights from dynamic neutron and X-ray scattering, Journal of Polymer Science. 60 (2022) 1130–1150, https://doi.org/10.1002/pol.20210320.

[27] Y.Y. Zhang, Y.T. Gu, Mechanical properties of graphene: Effects of layer number, temperature and isotope, Comput Mater Sci. 71 (2013) 197–200, https://doi.org/10.1016/j.commatsci.2013.01.032.

[28] Y. Shen, H. Wu, Interlayer shear effect on multilayer graphene subjected to bending, Appl Phys Lett. 100 (2012) 1–4, https://doi.org/10.1063/1.3693390.

[29] M.T. Masood, E.L. Papadopoulou, J.A. Heredia-Guerrero, I.S. Bayer, A. Athanassiou, L. Ceseracciu, Graphene and polytetrafluoroethylene synergistically improve the tribological properties and adhesion of nylon 66 coatings, Carbon N Y. 123 (2017) 26–33, https://doi.org/10.1016/j.carbon.2017.07.026.

[30] M. Sabzi, L. Jiang, N. Nikfarjam, Graphene nanoplatelets as rheology modifiers for polylactic acid: Graphene aspect-ratio-dependent nonlinear rheological behavior, Ind Eng Chem Res. 54 (2015) 8175–8182, https://doi.org/10.1021/acs.iecr.5b01863.

[31] S. Colonna, D. Battegazzore, M. Eleuteri, R. Arrigo, A. Fina, Properties of graphene-related materials controlling the thermal conductivity of their polymer nanocomposites, Nanomaterials. 10 (2020) 1–20, https://doi.org/10.3390/nano10112167.

[32] S. Jain, J.G.P. Goossens, G.W.M. Peters, M. van Duin, P.J. Lemstra, Strong decrease in viscosity of nanoparticle-filled polymer melts through selective adsorption, Soft Matter. 4 (2008) 1848–1854, https://doi.org/10.1039/b802905a.

[33] N.K. Kwon, H. Kim, T.J. Shin, K. Saalwächter, J. Park, S.Y. Kim, Control of Particle Dispersion with Autophobic Dewetting in Polymer Nanocomposites, Macromolecules. 53 (2020) 4836–4844, https://doi.org/10.1021/acs.macromol.0c00190.

[34] S.K. Kumar, N. Jouault, B. Benicewicz, T. Neely, Nanocomposites with polymer grafted nanoparticles, Macromolecules. 46 (2013) 3199–3214, https://doi.org/10.1021/ma4001385.

[35] M. Giovino, E. Buenning, A. Jimenez, S.K. Kumar, L. Schadler, Polymer Grafted Nanoparticle Viscosity Modifiers, Macromol Chem Phys 220 (7) (2019) 1800543, https://doi.org/10.1002/macp.201800543.

[36] L. Bai, S. He, J.W. Fruehwirth, A. Stein, C.W. Macosko, X. Cheng, Localizing graphene at the interface of cocontinuous polymer blends: Morphology, rheology, and conductivity of cocontinuous conductive polymer composites, J Rheol. 61 (2017) 575–587, https://doi.org/10.1122/1.4982702.

[37] R. Altobelli, M. Salzano de Luna, G. Filippone, Interfacial crowding of nanoplatelets in co-continuous polymer blends: assembly, elasticity and structure of the interfacial nanoparticle network, Soft Matter. 13 (2017) 6465–6473, https://doi.org/10.1039/C7SM01119A.

[38] J. Plattier, L. Benyahia, M. Dorget, F. Niepceron, J.F. Tassin, Viscosity-induced filler localisation in immiscible polymer blends, Polymer. 59 (2015) 260–269, https://doi.org/10.1016/j.polymer.2014.12.044.

[39] M. Hadaeghnia, S. Ahmadi, I. Ghasemi, P.M. Wood-Adams, Manipulating the morphology of PA6/POE blends using graphene to achieve balanced electrical and mechanical properties, Compos Sci Technol. 200 (2020), 108412, https://doi.org/10.1016/j.compscitech.2020.108412.

[40] A.L. Persson, H. Bertilsson, Viscosity difference as distributing factor in selective absorption of aluminium borate whiskers in immiscible polymer blends, Polymer 39 (23) (1998) 5633–5642, https://doi.org/10.1016/S0032-3861(98)00096-2.

[41] D.R. Paul, J.W. Barlow, Polymer Blends, Journal of Macromolecular Science, Part C 18 (1980) 109–168, https://doi.org/10.1080/00222358008080917.
[42] R. Salehiyan, M. Nofar, K. Malkappa, S.S. Ray, Effect of nanofillers characteristics and their selective localization on morphology development and rheological properties of melt-processed polylactide/poly(butylene adipate-co-terephthalate) blend composites, Polym Eng Sci. 60 (2020) 2749–2760, https://doi.org/10.1002/pen.25505.
[43] M. Nofar, R. Salehiyan, S.S. Ray, Influence of nanoparticles and their selective localization on the structure and properties of polylactide-based blend nanocomposites, Compos B Eng 215 (2021) 108845, https://doi.org/10.1016/j.compositesb.2021.108845.